Biochemical and Biophysical Research Communications 464 (2015) 1060–1065

Contents lists available at ScienceDirect

Biochemical and Biophysical Research Communications

journal homepage: www.elsevier.com/locate/ybbrc

Quantification of Ataxin-3 and Ataxin-7 aggregates formed *in vivo* in *Drosophila* reveals a threshold of aggregated polyglutamine proteins associated with cellular toxicity

Gérald Vinatier, Jean-Marc Corsi, Bernard Mignotte, Sébastien Gaumer*

Laboratoire de Génétique et Biologie Cellulaire, EA4589, Université Versailles-St-Quentin-en-Yvelines, Ecole Pratique des Hautes Etudes, 2 rue de la source de la Bièvre, 78180 Montigny-le-Bx, France

ARTICLE INFO

Article history:
Received 10 July 2015
Accepted 14 July 2015
Available online 22 July 2015

Keywords:
Polyglutamine disease
Protein aggregates
SCA3
SCA7
Drosophila melanogaster

ABSTRACT

Polyglutamine diseases are nine dominantly inherited neurodegenerative pathologies caused by the expansion of a polyglutamine domain in a protein responsible for the disease. This expansion leads to protein aggregation, inclusion formation and toxicity. Despite numerous studies focusing on the subject, whether soluble polyglutamine proteins are responsible for toxicity or not remains debated. To focus on this matter, we evaluated the level of soluble and insoluble truncated pathological Ataxin-3 *in vivo* in *Drosophila*, in presence or absence of two suppressors (*i.e.* Hsp70 and non-pathological Ataxin-3) and along aging. Suppressing truncated Ataxin-3-induced toxicity resulted in a lowered level of aggregated polyglutamine protein. Interestingly, aggregates accumulated as flies aged and reached a maximum level when cell death was detected. Our results were similar with two other pathological polyglutamine proteins, namely truncated Ataxin-7 and full-length Ataxin-3. Our data suggest that accumulation of insoluble aggregates beyond a critical threshold could be responsible for toxicity.

1. Introduction

Polyglutamine (PolyQ) diseases are fatal dominantly inherited neurodegenerative disorders provoked by the expansion of a polyQ domain in a disease-specific protein prone to aggregate. With Huntington's disease, Spinobulbar Muscular Atrophy, Dentatorubral Pallidoluysian Atrophy, Spinocerebellar Ataxia (SCA) type 1, 2, 6 and 17, SCA3 and SCA7 are two of the nine polyQ diseases identified to this date. When the size of their polyQ domain exceeds a threshold of 54 glutamines for the Atx3 protein or 36 for the Atx7 protein, patients respectively develop the SCA3 or SCA7 disease [1].

A common feature to polyQ diseases is the presence of inclusions detectable by microscopy on histological brain slices from patients or in cellular and animal models. Inclusions are mainly nuclear [2,3] and contain numerous proteins, including the polyQ protein responsible for the pathology and chaperone proteins such as Hsp70 [4]. Neither the conformation nor the oligomerization states of the pathological polyQ proteins can be fully characterized *in vivo* whether inside or outside inclusions. Therefore the link between aggregates and inclusions remains unclear.

Recent studies have focused on oligomers that can be formed by elongated polyQ proteins. Oligomers have been detected both *in vitro* and *in vivo* as multiple different oligomeric conformations [5–8]. They can be considered as soluble [6,9] or insoluble [8] but the notion of solubility is not defined on common grounds. Depending on the study, soluble oligomers are either toxic [10,11] or not [12], and reciprocally, insoluble oligomers can be either toxic [13] or not [8].

In the present work we sought to investigate the toxicity of the SDS-soluble or -insoluble species of Atx3 and Atx7 polyQ proteins formed *in vivo*.

2. Materials and methods

2.1. Fly genetics and phenotype observation

All crosses were grown at 25 °C or 19 °C on standard medium, which was changed every other day. Glass-Mediated Response-GAL4 (GMR-gal4) was used as a GAL4 driver. *Drosophila* eyes were photographed with a Leica MZFL III microscope.

* Corresponding author.
E-mail address: sebastien.gaumer@uvsq.fr (S. Gaumer).

http://dx.doi.org/10.1016/j.bbrc.2015.07.071
0006-291X/

2.2. Western and dot blotting

Twenty male and twenty female flies were sacrificed in liquid nitrogen. Their heads were crushed in denaturing buffer (TE pH 8.5; 2% SDS, 0.05M DTT; 10 μM Protease Inhibitor Cocktail AEBSF, Roche) and incubated at 96 °C for 12 min. Part of the protein extracts was dot blotted on a nitrocellulose membrane (Schleicher and Schuell, Whatman, OPTITRAN BA-S85, 0.45 μm) without aspiration to quantify the SDS-insoluble fraction named hereafter aggregates. Another part of the same extracts was separated by Western Blot to quantify the SDS-soluble fraction on NuPAGE 4–12% Bis-Tris polyacrylamide gels following standard protocols [14]. Immunoreactive bands were detected by ImmobilonTM western Chemoluminescent HRP Substrate (Millipore) and chemoluminescent signals were quantified with a BioRad Chemidoc™ XRS+ or Molecular Imager® System GS505, allowing saturation-free measures. The glass protein was used as a loading control, since it is specifically expressed in the cells of interest.

Western blot quantifications are often considered as non-linear. To make sure that our western blotting conditions allow linearity of protein quantifications, we compared the signals observed for Glass immunodetection with two-fold dilutions of 54 independent samples. The average ratio between dilution quantifications was exactly equal to 2 with a standard error of 0.12. Therefore, our protocol allows linear quantification of SDS-soluble proteins.

2.3. Antibodies and reagents

Primary antibodies used were mouse anti-Myc (9E10, 1/1000, Developmental Studies Hybridoma Bank), rabbit anti-Myc (1/100, #2272, Cell Signaling), mouse anti-Ha (Ha.11 16B12, 1/5000, Eurogentec), rabbit anti-Atx7 (PA1-749, 1/400, OZYME), mouse anti-Glass (9B2.1, 1/250, Developmental Studies Hybridoma Bank), Horseradish peroxidase conjugated secondary antibodies (1/10000, Jackson ImmunoResearch).

2.4. Statistical analyses

Each experiment was realized at least thrice independently and two dilutions of the samples were used to verify the linearity of the quantification process. The quantitative results were analyzed by ANOVA. To work on more normal data, we applied a log transformation to the measures or a square root transformation when focusing on the threshold of protein levels involved in triggering cell death.

3. Results

3.1. Quantification of SDS-soluble and -insoluble Atx proteins by western and dot blotting

The definition of protein aggregates often varies. They are defined in our study as oligomers that resist boiling in a 2% SDS reducing solution. Aggregate quantities are often evaluated from the amount of proteins trapped at the top of western blots. However, only small aggregates can enter stacking gels, while large aggregates cannot. An alternative method to quantify aggregates is dot blotting. To compare the accuracy of western and dot blotting quantifications of protein aggregates, we first used a SCA3 model based on the expression of truncated human Atx3 (Atx3tr, Fig. S1). Driven by the UAS-gal4 expression system and using the GMR-gal4 driver, the transgene was expressed in all cells posterior to the morphogenetic furrow in the eye tissue, including photoreceptor neurons. We compared the ratio of signals detected for two dilutions of forty independent samples with both techniques. The average ratio was similar for western and dot blots. Interestingly, the variance of the ratio was 2.75 times higher with western blots than with dot blots (Fig. S2, F test: $p < 2 \cdot 10^{-3}$). Therefore, dot blotting is more reproducible for aggregate quantification than western blotting.

Relative soluble and aggregated Atx protein levels per cell were determined in the following experiments by normalizing Atx levels with the Glass protein level. *Glass* gene expression is restricted to few cells of the central nervous system and to the differentiated cells of the eye tissue [15]. As Glass directly controls the expression of *GAL4* with the GMR-gal4 construct used to drive the expression of the different transgenes in this study, Glass levels roughly characterize the number of Atx-expressing cells that remain alive. Hence, we used Glass levels to normalize the quantity of Atx proteins per Atx-expressing cell, rather than usual loading controls (such as tubulin), which would have evaluated the amount of Atx proteins per cell, whether cells expressed Atx or not.

3.2. Aggregated truncated Atx3 protein level is correlated with toxicity

As described by the group of Nancy Bonini [16,17], while the non-pathological Atx3Q27tr that carries a repeat of 27 glutamines does not induce toxicity, pathological Atx3Q78tr induces cell death (Fig. S3A–B). The Atx3Q78tr model is of particular interest since truncated forms of Atx3 can be observed *in vivo* [18,19] and could be more relevant for the study of polyQ protein-induced toxicity since they reveal more toxic than the corresponding full-length protein [20–24].

Atx3Q78tr-induced apoptosis is opposed by human Hsp70 and non-pathological full-length Atx3Q27 as observed by cross-sectioning [16,17] and through a loss of pigmentation of the eye (Fig. S3B) that has been shown to be due to the death of pigment cells [25]. Interestingly, cell death is not fully suppressed by Hsp70 and Atx3Q27, but is only slowed down since loss of pigmentation appeared in 45-day-old flies (Fig. S3B). As shown in Fig. S3E, the effect of suppressors is not due to GAL4 titration.

To better understand the relationship between aggregation and toxicity, we compared the amount of aggregated and SDS-soluble Atx3Q78tr in different genetic backgrounds that modulate toxicity. Suppressing Atx3Q78tr-induced toxicity decreased the quantity of aggregated Atx3Q78tr (Fig. 1A, left panel) without affecting its soluble level (Fig. 1A, right panel) (Representative western and dot blots are shown in Fig. S4A). The UAS-GAL4 system is temperature-sensitive and decreasing the temperature lowers the expression of transgenes. To reduce the levels of Atx3Q78tr and thus toxicity that was extreme and only left few cells to study, we lowered the temperature at which flies were raised from 25 °C to 19 °C. The quantity of aggregated Atx3Q78tr remained reduced by both Atx3Q27 and Hsp70 but these suppressors also significantly reduced the soluble Atx3Q78tr level (Fig. 1B and Fig. S4B). Globally, the data obtained at 25 °C and 19 °C suggest that Atx3Q78tr soluble levels are not linked to the toxicity whereas its aggregated level could be.

3.3. A threshold of aggregated polyQ protein characterizes cell death onset

As previously indicated, phenotypes aggravate while flies producing Atx3Q78tr age. We thus wondered whether the level of aggregates of pathological polyQ proteins increased with aging. Interestingly, neither aggregated nor soluble levels of Atx3Q78tr significantly changed between 2- and 30-day-old flies (Fig. 1C, black bars and Fig. S5A). As assessed by eye degeneration, toxicity was already detectable in two-day-old Atx3Q78tr-expressing flies

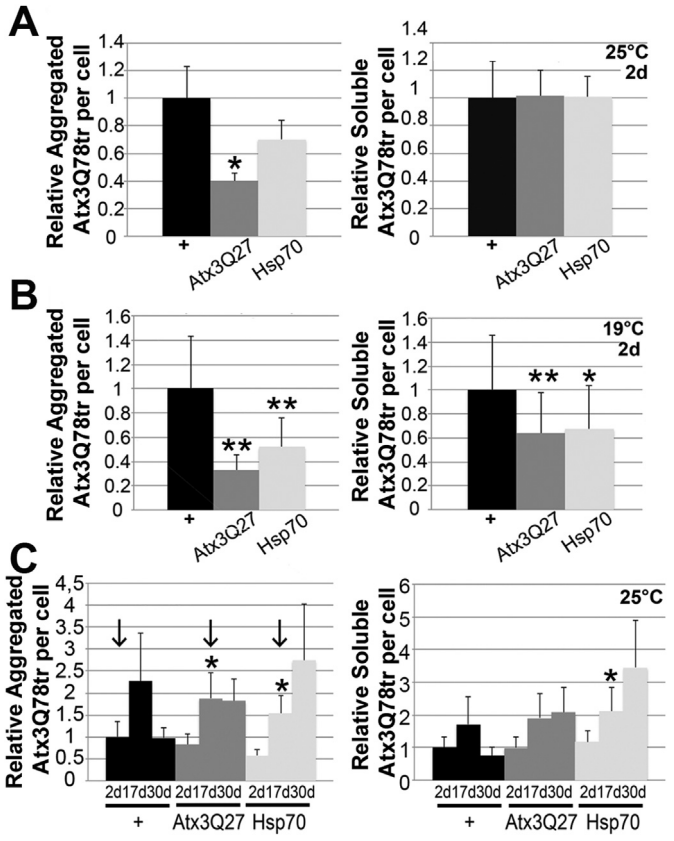

Fig. 1. Effects of Hsp70, Atx3Q27 and aging on Atx3Q78tr protein levels. Relative Atx3Q78tr cellular levels measured in flies raised at 25 °C (A,C) or 19 °C (B) in the absence (black) or presence of Atx3Q27 (dark grey) or Hsp70 (light grey) transgene expression. Flies were two-day-old (A, B) or aged for 2, 17 or 30 days (C). The relative aggregated Atx3Q78tr level (left histograms) is the ratio between the dot blot signal and the glass signal. The relative soluble Atx3Q78tr level (right histograms) is the ratio between the western blot signal and the glass signal. (A, B) Statistical difference with the first condition on the histogram is indicated by * when $p < 5\%$ and ** when $p < 1\%$ (ANOVA). (C) Statistical difference with the preceding time is indicated by * (ANOVA, $p < 5\%$). Arrows indicate the onset of eye degeneration revealed by the loss of pigment cells. Genotypes: *GMR-gal4*/+; *UAS-atx3Q78tr*/+ (+), *GMR-gal4*/*UAS-atx3Q27*; *UAS-atx3Q78tr*/+ (Atx3Q27), *GMR-gal4*/*UAS-hsp70*; *UAS-atx3Q78tr*/+ (Hsp70).

(arrow in Fig. 1C). These data might suggest that aging has no effect on the levels of aggregated and soluble AtxQ78tr once degeneration occurs.

When looking at the effect of aging in flies co-expressing one of the suppressors with pathological Atx3, the level of aggregated Atx protein increased until cell death appeared in 17-day-old flies (Fig. 1C, light and dark grey bars). On the contrary, the level of SDS-soluble Atx3Q78tr remained statistically unchanged as flies aged in the presence of Atx3Q27, while it increased in the presence of Hsp70. Therefore, cell death detection seems associated to a maximum in aggregated levels of Atx3Q78tr.

3.4. Full-length Atx3 and truncated Atx7 behave as truncated Atx3

To confirm these results, we used a second model of SCA3 disease established in *Drosophila, i.e.* a pathological full-length form of the Atx3 protein, which contains a 78-glutamine-long domain (Fig. S1). As its truncated form, full-length Atx3Q78 led to degeneration that was visible in emerging adults and progressed as flies aged but it appeared less toxic than Atx3Q78tr (Fig. S3B–C). Similarly to what was observed with Atx3Q78tr, both suppressors mitigated Atx3Q78-induced eye degeneration ([17] and Fig. S3C).

We only tested the effect of Hsp70 in the dot blot quantification experiments since Atx3Q27 and Atx3Q78 bear the same Myc tag. Similarly to our observations with Atx3Q78tr, Hsp70 was able to decrease the quantity of aggregated Atx3Q78 (Fig. 2A, left panel and Fig. S4C).

A striking difference between the truncated and full-length pathological forms of Atx3 lied in the levels of soluble pathological protein (Fig. 2A, right panel). Soluble Atx3Q78 levels increased in the presence of Hsp70, while Hsp70 did not affect (Fig. 1A, right panel) or decreased (Fig. 1B, right panel) soluble Atx3Q78tr levels. These results highlight a discrepancy between the levels of pathological Atx3 that remains soluble and cytotoxicity.

When flies were raised at 19 °C, the lower expression of *Atx3Q78* did not lead to significant cell death when looking at the external eye structure (data not shown). In these conditions, Hsp70 did not significantly affect the level of soluble Atx3Q78 but decreased the aggregated Atx3Q78 levels (Fig. 2B and Fig. S4D).

Neither aggregated nor SDS-soluble Atx3Q78 levels were affected by aging in the absence of suppressor (Fig. 2C, black bars and Fig. S5B). Hsp70 expression led to an increase in aggregated and a decrease in SDS-soluble Atx3Q78 in 17-day-old flies (Fig. 2C,

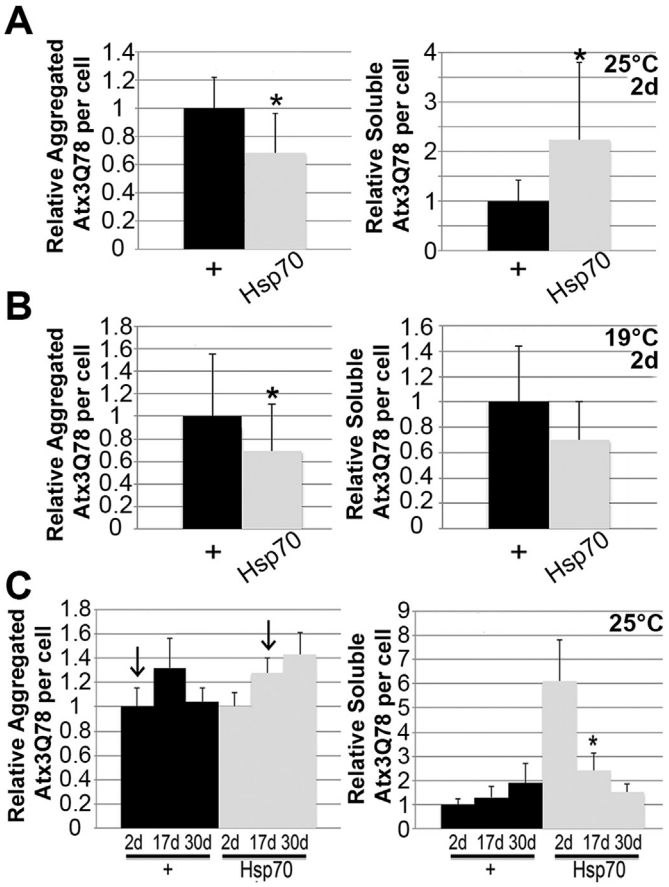

Fig. 2. Effects of Hsp70 and aging on Atx3Q78 and protein levels. Relative Atx3Q78 cellular levels measured in flies raised at 25 °C (A, C) or 19 °C (B) in the absence (black) or presence (grey) of Hsp70 transgene expression. Flies were two-day-old (A, B) or aged for 2, 17 or 30 days (C). The relative aggregated Atx3Q78 level (left histograms) is the ratio between the dot blot signal and the glass signal. The relative soluble Atx3Q78 level (right histograms) is the ratio between the western blot signal and the glass signal. (A, B) Statistical difference with the first condition on the histogram is indicated by * when $p < 5\%$ (ANOVA). (C) Statistical difference with the preceding time is indicated by * (ANOVA, $p < 5\%$). Arrows indicate the onset of eye degeneration revealed by the loss of pigment cells. Genotypes: *GMR-gal4*/+; *UAS-atx3Q78*/+ (+), *GMR-gal4*/*UAS-hsp70*; *UAS-atx3Q78*/+ (Hsp70).

grey bars), *i.e.* the age at which cell death is detected. No significant change of aggregated or soluble cellular levels of Atx3Q78 was observed after 17 days of aging. Therefore, as observed with Atx3Q78tr, aggregated levels of Atx3Q78 are unaffected once degeneration can be detected.

To test if our results were specific of Atx3 forms, we used a model of SCA7 based on the expression of a truncated form of the protein held responsible for this disease when carrying a long polyQ domain, Atx7Q102tr (Fig. S1). This protein does not share sequence similarities with Atx3 besides its polyQ domain. Atx7Q102tr did not induce any detectable external phenotype before flies were 15-day-old (Fig. S3D). As flies aged, the weak loss of pigmentation revealing loss of pigment cells at the border of the eye spread throughout the tissue by 45 days of age (Fig. S3D). Even though Atx3Q27 delayed the age of onset of degeneration induced by pathological Atx7, it did not entirely suppress degeneration as flies aged (Fig. S3D).

Interestingly, Atx7Q102tr behaved as pathological Atx3 in the presence of a suppressor of polyQ toxicity at 25 °C. Indeed, the aggregated cellular level of Atx7Q102tr was reduced by Atx3Q27 both in the presence or absence of toxicity respectively in 17- or 2-day-old flies (Fig. 3A and B, left panels), while its SDS-soluble level either increased or remained unchanged (Fig. 3A and B, right panels and Fig. S4E–F).

We tested whether Atx3Q27 delayed an increase in aggregated Atx7Q102tr, as observed with pathological Atx3. Indeed, Atx3Q27 delayed both eye degeneration and the maximal aggregated level of Atx7Q102tr per cell to 30-day-old flies (Fig. 3C and Fig. S5C). Once again, SDS-soluble levels of Atx7Q102tr were not correlated with toxicity while aggregated levels increased until cell death could be detected.

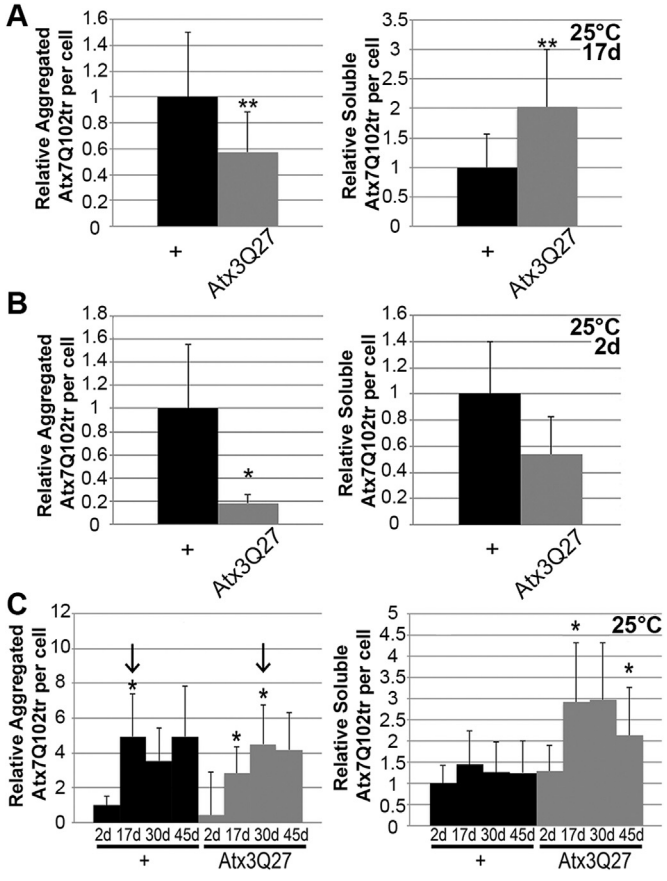

Fig. 3. Effects of Atx3Q27 and aging on Atx7Q102tr protein levels. Relative Atx7Q102tr cellular levels measured in flies raised at 25 °C in the absence (black) or presence of Atx3Q27 (grey). Flies were 17- (A), 2- (B) or 2-, 17-, 30- or 45-day-old (C). The relative aggregated Atx7Q102tr level (left histograms) is the ratio between the dot blot signal and the glass signal. The relative soluble Atx7Q102tr level (right histograms) is the ratio between the western blot signal and the glass signal. (A, B) Statistical difference with the first condition on the histogram is indicated by * when $p < 5\%$ and ** when $p < 1\%$ (ANOVA). (C) Statistical difference with the preceding time is indicated by * (ANOVA, $p < 5\%$). Arrows indicate the onset of eye degeneration revealed by the loss of pigment cells. Genotypes: *GMR-gal4*/+;*UAS-atx7Q102tr*/+ (+), *GMR-gal4*/*UAS-atx3-Q27*;*UAS-atx7Q102tr*/+ (Atx3Q27).

4. Discussion

Characterizing the toxic species among the monomers, small or large oligomers, fibrils, inclusions, soluble and insoluble forms of polyQ proteins has been a major goal in the research on polyQ diseases but the means, models and definitions vary from a study to another. We chose to focus on solubility in a denaturing and reducing environment classically found in SDS-PAGE. To minimize SDS-insoluble aggregate loss, we quantified aggregated polyQ proteins by dot blotting and SDS-soluble polyQ proteins by western blotting. We worked on three *in vivo* models of two different polyQ diseases and quantified relative cellular levels of the different polyQ proteins.

Our data indicate that suppressing toxicity in the three models does not allow establishing any link between toxicity and soluble levels of polyQ proteins. On the opposite, the two suppressors consistently reduced aggregated polyQ protein levels. Therefore, aggregates seem to be the toxic form of polyQ proteins as inferred by Nguyen et al. on a mice model of SCA3 [26]. However, toxicity has been much more related to soluble forms of polyQ proteins than to their insoluble forms [6,11]. Our results could be reconciled with this part of the literature if oligomers that have been characterized as soluble by other methods were insoluble according to our criteria. Interestingly, Tonoki et al. suggest that transiently expressed Atx3Q78tr in aged individuals displays higher toxicity and a higher solubility in SDS than Axtx3Q78tr expressed in younger flies [27]. The discrepancy between our two studies could

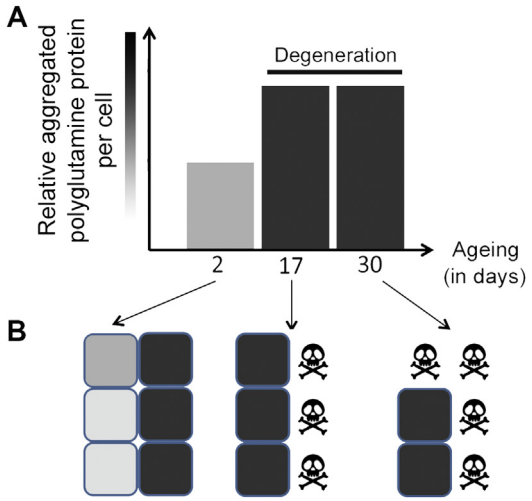

Fig. 4. Hypothetical model of a cell death onset associated with an aggregated polyglutamine protein threshold during aging. (A) Typical schematic evolution of relative aggregated polyQ protein level per cell in 2-, 17- and 30-day-old flies. Degeneration is associated with a stability of the cellular level of aggregated polyQ protein. (B) Model of evolution of the polyglutamine protein level in a group of cells. Each square represents a cell. The aggregated polyQ protein level varies between cells. In young flies with low levels of polyQ proteins (light gray) no cell death is observed. During aging, cellular polyglutamine protein levels increase until reaching a critical threshold (shown in dark gray) that leads to cell death (shown as a skull and crossbones).

rely on a difference in the transgene onset of expression, which could result in distinct seedings, leading to self-propagating amyloid forms characterized by specific conformations as described for prion proteins [28,29].

When cell death did not occur at the emergence of adult *Drosophila* because of either the expression level, the presence of a suppressor or the polyQ model, aggregates accumulated until cell death could be detected. We interpret this threshold of aggregated protein levels as the cellular aggregated protein lethal dose (Fig. 4). Supporting this result, different studies of Huntington's disease led on a mouse model and *in cellulo* showed that aggregates could be detected before any measurable toxic phenotype [30,31].

The only other study on the SCA7 *Drosophila* model showed a deleterious effect of truncated Atx7 on neurons resulting in a shortened lifespan and a locomotor dysfunction [14]. By expressing the same truncated Atx7 in the eye tissue, we could observe progressive degeneration of the eye as observed in the human pathogenesis, thereby highlighting the interest of this model to study the SCA7 disease in *Drosophila*.

In conclusion, our models of Atx7 and Atx3, which mimic the progressive accumulation of aggregates observed in patients during aging, support the hypothesis of a critical threshold of aggregated proteins associated with the induction of toxicity.

Acknowledgments

This article is dedicated to the memory of Didier Contamine who initiated this study and Evelyne Maillier who participated to some of these experiments. We would like to thank Hervé Tricoire and Nancy Bonini respectively for SCA7 and SCA3 transgenic models. Transgenic flies expressing hsp70, hsc4, hsc3, puc were provided by the Bloomington Drosophila Resource Center. The bsk$^{5680R-2}$ RNAi line was supplied by the National Institute of Genetics. We are thankful to Pierre Gandille, Alyssa Carré-Mlouka, Isabelle Brun-Heath, Yohan Demay for scientific discussions. We are grateful to Giovanni Stevanin, Sandro Alves and Sébastien Szuplewski for careful reading of the manuscript.

Transparency document

Transparency document related to this article can be found online at http://dx.doi.org/10.1016/j.bbrc.2015.07.071.

Appendix A. Supplementary data

Supplementary data related to this article can be found at http://dx.doi.org/10.1016/j.bbrc.2015.07.071

References

[1] C.A. Matos, S. de Macedo-Ribeiro, A.L. Carvalho, Polyglutamine diseases: the special case of ataxin-3 and Machado-Joseph disease, Prog. Neurobiol. 95 (2011) 26–48.
[2] S.W. Davies, M. Turmaine, B.A. Cozens, M. DiFiglia, A.H. Sharp, C.A. Ross, E. Scherzinger, E.E. Wanker, L. Mangiarini, G.P. Bates, Formation of neuronal intranuclear inclusions underlies the neurological dysfunction in mice transgenic for the HD mutation, Cell 90 (1997) 537–548.
[3] A. Lunkes, J.L. Mandel, Polyglutamines, nuclear inclusions and neurodegeneration, Nat. Med. 3 (1997) 1201–1202.
[4] M. Koike, J. Fukushi, Y. Ichinohe, N. Higashimae, M. Fujishiro, C. Sasaki, M. Yamaguchi, T. Uchihara, S. Yagishita, H. Ohizumi, S. Hori, A. Kakizuka, Valosin-containing protein (VCP) in novel feedback machinery between abnormal protein accumulation and transcriptional suppression, J. Biol. Chem. 285 (2010) 21736–21749.
[5] J. Legleiter, E. Mitchell, G.P. Lotz, E. Sapp, C. Ng, M. DiFiglia, L.M. Thompson, P.J. Muchowski, Mutant huntingtin fragments form oligomers in a polyglutamine length-dependent manner in vitro and in vivo, J. Biol. Chem. 285 (2010) 14777–14790.
[6] M. Li, E.S. Chevalier-Larsen, D.E. Merry, M.I. Diamond, Soluble androgen receptor oligomers underlie pathology in a mouse model of spinobulbar muscular atrophy, J. Biol. Chem. 282 (2007) 3157–3164.
[7] M.A. Olshina, L.M. Angley, Y.M. Ramdzan, J. Tang, M.F. Bailey, A.F. Hill, D.M. Hatters, Tracking mutant huntingtin aggregation kinetics in cells reveals three major populations that include an invariant oligomer pool, J. Biol. Chem. 285 (2010) 21807–21816.
[8] S.L. Wong, W.M. Chan, H.Y. Chan, Sodium dodecyl sulfate-insoluble oligomers are involved in polyglutamine degeneration, FASEB J. 22 (2008) 3348–3357.
[9] T. Takahashi, S. Katada, O. Onodera, Polyglutamine diseases: where does toxicity come from? what is toxicity? where are we going? J. Mol. Cell Biol. 2 (2010) 180–191.
[10] A. Demuro, E. Mina, R. Kayed, S.C. Milton, I. Parker, C.G. Glabe, Calcium dysregulation and membrane disruption as a ubiquitous neurotoxic mechanism of soluble amyloid oligomers, J. Biol. Chem. 280 (2005) 17294–17300.
[11] T. Takahashi, S. Kikuchi, S. Katada, Y. Nagai, M. Nishizawa, O. Onodera, Soluble polyglutamine oligomers formed prior to inclusion body formation are cytotoxic, Hum. Mol. Genet. 17 (2008) 345–356.
[12] C. Behrends, C.A. Langer, R. Boteva, U.M. Bottcher, M.J. Stemp, G. Schaffar, B.V. Rao, A. Giese, H. Kretzschmar, K. Siegers, F.U. Hartl, Chaperonin TRiC promotes the assembly of polyQ expansion proteins into nontoxic oligomers, Mol. Cell 23 (2006) 887–897.
[13] A. Wyttenbach, S. Hands, M.A. King, K. Lipkow, A.M. Tolkovsky, Amelioration of protein misfolding disease by rapamycin: translation or autophagy? Autophagy 4 (2008) 542–545.
[14] M. Latouche, C. Lasbleiz, E. Martin, V. Monnier, T. Debeir, A. Mouatt-Prigent, M.P. Muriel, L. Morel, M. Ruberg, A. Brice, G. Stevanin, H. Tricoire, A conditional pan-neuronal *Drosophila* model of spinocerebellar ataxia 7 with a reversible adult phenotype suitable for identifying modifier genes, J. Neurosci. 27 (2007) 2483–2492.
[15] K. Moses, G.M. Rubin, Glass encodes a site-specific DNA-binding protein that is regulated in response to positional signals in the developing *Drosophila* eye, Genes Dev. 5 (1991) 583–593.
[16] J.M. Warrick, H.Y. Chan, G.L. Gray-Board, Y. Chai, H.L. Paulson, N.M. Bonini, Suppression of polyglutamine-mediated neurodegeneration in *Drosophila* by the molecular chaperone HSP70, Nat. Genet. 23 (1999) 425–428.
[17] J.M. Warrick, L.M. Morabito, J. Bilen, B. Gordesky-Gold, L.Z. Faust, H.L. Paulson, N.M. Bonini, Ataxin-3 suppresses polyglutamine neurodegeneration in *Drosophila* by a ubiquitin-associated mechanism, Mol. Cell 18 (2005) 37–48.
[18] D. Goti, S.M. Katzen, J. Mez, N. Kurtis, J. Kiluk, L. Ben-Haiem, N.A. Jenkins, N.G. Copeland, A. Kakizuka, A.H. Sharp, C.A. Ross, P.R. Mouton, V. Colomer, A mutant ataxin-3 putative-cleavage fragment in brains of Machado-Joseph disease patients and transgenic mice is cytotoxic above a critical concentration, J. Neurosci. 24 (2004) 10266–10279.
[19] G. Yvert, K.S. Lindenberg, D. Devys, D. Helmlinger, G.B. Landwehrmeyer, J.L. Mandel, SCA7 mouse models show selective stabilization of mutant ataxin-7 and similar cellular responses in different neuronal cell types, Hum. Mol. Genet. 10 (2001) 1679–1692.
[20] A. Haacke, S.A. Broadley, R. Boteva, N. Tzvetkov, F.U. Hartl, P. Breuer, Proteolytic cleavage of polyglutamine-expanded ataxin-3 is critical for aggregation and sequestration of non-expanded ataxin-3, Hum. Mol. Genet. 15 (2006) 555–568.
[21] J. Hubener, J.J. Weber, C. Richter, L. Honold, A. Weiss, F. Murad, P. Breuer, U. Wullner, P. Bellstedt, F. Paquet-Durand, J. Takano, T.C. Saido, O. Riess, H.P. Nguyen, Calpain-mediated ataxin-3 cleavage in the molecular pathogenesis of spinocerebellar ataxia type 3 (SCA3), Hum. Mol. Genet. 22 (2013) 508–518.
[22] J. Liman, S. Deeg, A. Voigt, H. Vossfeldt, C.P. Dohm, A. Karch, J. Weishaupt, J.B. Schulz, M. Bahr, P. Kermer, CDK5 protects from caspase-induced Ataxin-3 cleavage and neurodegeneration, J. Neurochem. 129 (2014) 1013–1023.
[23] A.T. Simoes, N. Goncalves, A. Koeppen, N. Deglon, S. Kugler, C.B. Duarte, L. Pereira de Almeida, Calpastatin-mediated inhibition of calpains in the mouse brain prevents mutant ataxin 3 proteolysis, nuclear localization and aggregation, relieving Machado-Joseph disease, Brain 135 (2012) 2428–2439.
[24] J.E. Young, L. Gouw, S. Propp, B.L. Sopher, J. Taylor, A. Lin, E. Hermel, A. Logvinova, S.F. Chen, S. Chen, D.E. Bredesen, R. Truant, L.J. Ptacek, A.R. La Spada, L.M. Ellerby, Proteolytic cleavage of ataxin-7 by caspase-7 modulates cellular toxicity and transcriptional dysregulation, J. Biol. Chem. 282 (2007) 30150–30160.
[25] J.M. Warrick, H.L. Paulson, G.L. Gray-Board, Q.T. Bui, K.H. Fischbeck, R.N. Pittman, N.M. Bonini, Expanded polyglutamine protein forms nuclear inclusions and causes neural degeneration in *Drosophila*, Cell 93 (1998) 939–949.
[26] H.P. Nguyen, J. Hubener, J.J. Weber, S. Grueninger, O. Riess, A. Weiss, Cerebellar soluble mutant ataxin-3 level decreases during disease progression in Spinocerebellar Ataxia Type 3 mice, PLoS One 8 (2013) e62043.
[27] A. Tonoki, E. Kuranaga, N. Ito, Y. Nekooki-Machida, M. Tanaka, M. Miura, Aging causes distinct characteristics of polyglutamine amyloids *in vivo*, Genes Cells 16 (2011) 557–564.
[28] R. Diaz-Avalos, C.Y. King, J. Wall, M. Simon, D.L. Caspar, Strain-specific morphologies of yeast prion amyloid fibrils, Proc. Natl. Acad. Sci. U. S. A. 102 (2005) 10165–10170.
[29] S. Hannaoui, L. Maatouk, N. Privat, E. Levavasseur, B.A. Faucheux, S. Haik, Prion propagation and toxicity occur in vitro with two-phase kinetics specific to strain and neuronal type, J. Virol. 87 (2013) 2535–2548.
[30] P. Koch, P. Breuer, M. Peitz, J. Jungverdorben, J. Kesavan, D. Poppe, J. Doerr,

J. Ladewig, J. Mertens, T. Tuting, P. Hoffmann, T. Klockgether, B.O. Evert, U. Wullner, O. Brustle, Excitation-induced ataxin-3 aggregation in neurons from patients with Machado-Joseph disease, Nature 480 (2011) 543–546.
[31] A. Weiss, C. Klein, B. Woodman, K. Sathasivam, M. Bibel, E. Regulier, G.P. Bates, P. Paganetti, Sensitive biochemical aggregate detection reveals aggregation onset before symptom development in cellular and murine models of Huntington's disease, J. Neurochem. 104 (2008) 846–858.